

## INFLUENCE OF OXIDATION NUMBER OF MANGANESE ON MAGNETIC PROPERTIES OF LEAD FREE PIEZOELECTRIC BNT CERAMICS

M. Q. AWAN<sup>ab\*</sup>, J. AHMAD<sup>a</sup>, A. BERLIE<sup>b,c</sup>, Y. LIU<sup>b</sup>

<sup>a</sup>SSS Laboratory, Department of Physics, Bahauddin Zakariya University, Multan 60800, Pakistan

<sup>b</sup>Research School of Chemistry, Australian National University, Canberra Act 2601, Australia

<sup>c</sup>ISIS Neutron and Muon Source, STFC Rutherford Appleton Laboratory, Harwell Science and Innovation Campus, Didcot, Oxfordshire OX11 0QX, United Kingdom

$\text{Bi}_{0.5}\text{Na}_{0.5}\text{Ti}_{1-x}\text{Mn}_x\text{O}_3$  ( $x = 0.00, 0.02, 0.05, 0.10, 0.15$ ) ceramics were synthesized by following a solid state reaction route, in which  $\text{Mn}^{4+}$  cations were supposed to substitute  $\text{Ti}^{4+}$  cations on the B-site. The site occupation and valence fluctuation of  $\text{Mn}^{2+/3+/4+}$  and  $\text{Ti}^{3+/4+}$  were characterized by X-ray Photoelectron Spectroscopy (XPS) and Electron Spin Resonance (ESR) for the BNTM-10 ceramics. Magnetization measurements were performed in a Superconducting Quantum Interference Device (SQUID) magnetometer under the condition of the field-cooled and zero field-cooled temperature for applied fields of 100 G and 1 kG. The results revealed a paramagnetic behaviour for the Mn-doped BNT at higher doping levels. This paramagnetism can be ascribed to the exchange of the coupling interaction between  $\text{Mn}^{3+/2+}$  ions and  $\text{Ti}^{4+}$  vacancy.

(Received October 4, 2017; Accepted January 12, 2018)

*Keywords:* Lead free piezoelectric materials, BNTM ceramics, Mn doping, Magnetism

### 1. Introduction

Lead-free piezoelectric materials have generated broad interest due to the potential hazards of lead-based (Pb) materials to human health and the ecological environment.  $\text{Bi}_{0.5}\text{Na}_{0.5}\text{TiO}_3$ -based solutions with a morphotropic phase boundary (MPB) are among the strongest candidates to replace traditional lead zirconate titanate [1-3] in the development of actuators and transducers [4, 5]. BNT has a perovskite structure at room temperature along with a rhombohedral symmetry. Its A-sites are simultaneously composed of the  $\text{Bi}^{3+}$  and  $\text{Na}^{+}$  bimetallic ions and the B-site occupies  $\text{Ti}^{4+}$  ions. In contrast to other lead-free piezoelectric materials, BNT demonstrates a stronger ferroelectric effect, with a high value of remnant polarization along with excellent magnetic properties. BNT also exhibits a comparatively higher Curie temperature (320 °C) due to its special crystal structure and chemical composition [1, 6]. Although, its properties are reasonable for practical application, these values are still lower than that of lead zirconate-titanate (PZT).

The doping of extrinsic ions into the A/B site of BNT is considered a promising technique for improving the effective physical performances of this material. For example, manganese (Mn) ions are normally selected to enhance the piezoelectric properties of BNT ceramics [7, 8]. The incorporation of these ions also alters the magnetic properties or induces large recoverable electrostrain in the doped material, such as in Mn-doped  $\text{BaTiO}_3$  ceramics [9, 10]. In the periodic table, the Mn element is predominantly appealing as it is situated in the middle of the 3d-subshell and demonstrate variable chemical valences. Moreover, Mn ions are commonly used as sintering additives for a wide variety of compounds, to lower their sintering temperature and increase their

---

\* Corresponding author: a\_q\_khan1982@hotmail.com

density [11, 12]. Studies which focus on the improvement of the properties of BNT by Mn doping are very common. However, attention should also be directed at understanding the composition dependent responses of these solid solutions. In addition, the intrinsic relationship between the material properties and the doped crystal structure (average or local) should be thoroughly investigated.

Mn-doped BNT ceramics have been synthesized with high doping concentrations (up to 15 wt.% without phase segregation) with a chemical formula of  $\text{Bi}_{0.5}\text{Na}_{0.5}\text{Ti}_{1-x}\text{Mn}_x\text{O}_3$  ( $x=0.00, 0.02, 0.05, 0.10, 0.15$ ) in our recent work.  $\text{Mn}^{4+}$  cations were doped into the B-site by the replacement of some  $\text{Ti}^{4+}$  cations, based on the solid state reaction route. The results from extensive reports on A-site doping of BNT [13-17] often excludes results for B-site doping. To confirm the valance of Mn and its site occupation, current studies have utilized XPS and ESR data. Magnetic properties have also been presented in detail to elucidate the relationships between Mn substitution and performance.

## 2. Experimental Procedure

Manganese-doped  $\text{Bi}_{0.5}\text{Na}_{0.5}\text{TiO}_3$  with the chemical formula  $\text{Bi}_{0.5}\text{Na}_{0.5}\text{Ti}_{1-x}\text{Mn}_x\text{O}_3$  ( $x = 0.00, 0.02, 0.05, 0.10, \text{ and } 0.15$ ) were synthesized by the traditional solid state reaction route. The detailed synthesis process is elaborated in our recent work. The electric field dependent polarization (P-E) hysteresis loops were measured using a standard ferroelectric analyser (TF-2000). Poling of the samples was conducted using a DC field strength of 4–5 kV/mm in a silicon oil bath (80 °C, 20 min). The chemical valences of  $\text{Mn}^{2+}/\text{Mn}^{3+}/\text{Mn}^{4+}$  and  $\text{Ti}^{4+}/\text{Ti}^{3+}$  were determined by X-ray Photoelectron spectroscopy (XPS, Thermo ESCALAB 250Xi) and electron spin resonance (ESR, Bruker BioSpine EPR). The measurement of their magnetic properties was performed in a superconducting quantum interference device magnetometer (SQUID) at the field-cooled and zero field-cooled temperature for frequencies of 100 Hz and 1 kHz.

## 3. Results and discussion

### 3.1. Electron-Spin Resonance (ESR) Spectroscopy

Fig. 1 shows an electron spin resonance (ESR) spectrum for BNTM-10 at room temperature. The ESR spectrum was acquired at a 10 GHz spectrometer rating and performed on the grains of the investigated samples, compared to the empty tube. Resonance occurred at the magnetic field value  $H_r \approx 3240$  Oe, which corresponds to an effective Lande value of  $g \approx 2$  (for unpaired electrons). This can be attributed to spin-spin, spin-lattice, and/or spin-orbit interactions between  $\text{Mn}^{2+}$  and  $\text{Mn}^{3+}$  ions [18-21]. Although in the dopant oxide  $\text{MnO}_2$ , manganese is present as tetrahedral  $\text{Mn}^{4+}$ , an effective equilibrium of divalent  $\text{Mn}^{2+}$  and trivalent  $\text{Mn}^{3+}$  is present after 10% doping. The usual signatures from  $\text{Mn}^{4+}$  which would be typically observed for different g-values were not detected [22, 23]. The features at lower field values (around 2800 G) are due to paramagnetic oxygen. The other signal that exhibits more complex splitting around 3350 G is also confirmation of the presence of  $\text{Mn}^{2+}$  and the fine structure is due to the hyperfine coupling of the electronic and nuclear magnetism of this ion. It has been proposed that the Manganese charge state varies as a function of  $\text{O}_2$ . In the oxidizing limit, Mn isovalently substitutes for Ti as  $\text{Mn}^{4+}$ . Whereas in the reducing limit, Mn acts as an acceptor-type centre and replaces Ti as  $\text{Mn}^{2+}$  [24], where excess charge is compensated by the formation of oxygen vacancies. As  $\text{Mn}^{2+}$  and  $\text{Mn}^{3+}$  ions are substituting for higher valence ions, it is generally reported to form defect complexes. These are tentatively assigned to the di- and trivalent manganese functional centres in BNTM-10 to form  $(\text{MnTi}''-\text{V}_\text{o}^{\bullet\bullet})^\times$  and  $(\text{MnTi}'-\text{V}_\text{o}^{\bullet\bullet})^\circ$  defect complexes with oxygen vacancies [25-27]. It may be that ESR is of limited utility other than the identification of  $\text{Ti}^{3+}$  (or more specifically an ion with  $S = 1/2$  and  $L = 0$ , which we assign to  $\text{Ti}^{3+}$ ). From the XPS graphs, it is clear that we have  $\text{Ti}^{3+}$  and  $\text{Mn}^{2+}$  anyway. In addition, the magnetic data indicates the presence of a  $\text{Ti}^{3+}$  paramagnetic signal plus another unknown signal, which is likely due to the manganese.

Due to the size difference between  $\text{Ti}^{4+}$  (0.61 Å) and  $\text{Mn}^{4+}$  (0.53 Å), the Mn ions induce an internal chemical pressure within the crystal lattice [28]. This will result in the flattening of the free energy profile and increase the distortion of  $[(\text{Ti}, \text{Mn}) \text{O}_6]$  octahedral, (i.e. Jahn-Teller distortion), by lengthening the off-center displacement in the perovskite structure. The  $g$  value  $\sim 2$  corresponds to spin-spin interactions that are characteristics of the paramagnetic (PM) regime. This proves the presence of  $\text{Mn}^{2+}$  ions in the sample, which is in good agreement with the XRD based assessment in our recent paper. The dipole-dipole interaction, such as  $\text{Mn}^{2+} - \text{Mn}^{2+}$  is responsible for the resonance signals, similar to the case of magnetic resonance in perovskite maganites [29].

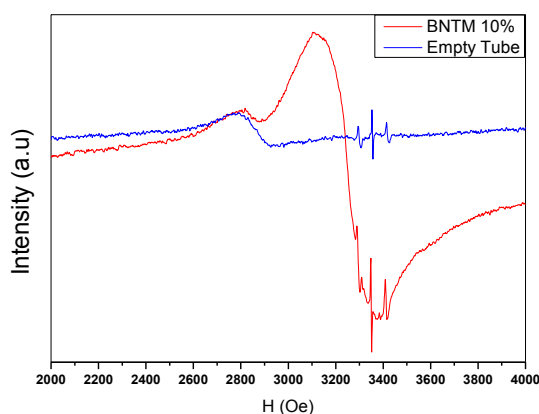


Fig. 1. ESR graph for BNTM-10 with red line showing the BNTM spectrum and blue line showing the spectrum of the empty tube.

### 3.2. X-ray photoelectron spectroscopy (XPS)

Fig. 2 shows the results of the X-ray photoelectron spectra performed on the BNTM-10 compound for  $\text{Ti}2p$ ,  $\text{Bi}4f$ ,  $\text{Mn}2p$ , and  $\text{Na}1s$ . To identify the oxidation state of the Mn dopant in the BNT ceramics, XPS is a very useful technique. Fig. 2 (a) shows the spectrum of  $\text{Ti}2p$ . The two major peaks  $\text{Ti}2p_{3/2}$  and  $\text{Ti}2p_{1/2}$  appear in the  $\text{Ti}2p$  spectrum at binding energies (BE) of 457.75 and 463.97 eV, respectively, and correspond to the angular momentum of the titanium electrons. The  $\text{Ti}2p_{3/2}$  peak is characterized by two peaks, where the smaller peak appears after the data is fitted at the BE of 458.48 eV. This peak is indicative of the presence of  $\text{Ti}^{3+}$ . Based on the shape of the  $\text{Ti}2p_{3/2}$ -A and  $\text{Ti}2p_{3/2}$ -B peaks and the fitting results, the conclusion can be drawn that  $\text{Ti}^{4+/3+}$  cations co-exist in the crystal lattice. Therefore, the positive charge of  $\text{V}_O^{\circ\circ}$  may be compensated by the reduction of  $\text{Ti}^{4+}$  to  $\text{Ti}^{3+}$ . This was also confirmed by the ESR spectrum. According to the charge potential model, the binding energy depends mainly on the average electron density of the element and the neighbouring environment [30].

Fig. 2 (d) shows the spectrum for  $\text{Na}1s$  and only one peak appears at the binding energy of 1071.77 eV, which is also disturbed by Mn doping. In the case of pure BNT, this peak appears at 1073.5 eV. The spectrum in Fig. 2 (b) shows that the two peaks which correspond to  $\text{Bi}4f_{7/2}$  and  $\text{Bi}4f_{5/2}$  for the  $\text{Bi}4f$  cation, appears at BE of 158.69 and 164.09 eV, respectively. No obvious change is observed in the  $\text{Bi}4f$  spectrum after higher level Mn doping. The difference in the BEs of  $\text{Na}^+$  and  $\text{Bi}^{3+}$  is the consequence of chemical disorder, which results in different effective electron densities of the elements.  $\text{Bi}^{3+}$  is under-bonded in BNT, with a deficiency compared to its ideal values which is much higher than the deficiency observed for  $\text{Na}^+$ . The  $\text{Bi}^{3+}$  ions displace and interact with oxygen, resulting in a much stronger Bi-O bond than the Na-O bond. Therefore, the BE of the  $\text{Na}^+$  ions is more sensitive to changes in the coordination environment.

From the Fig. 2, the difference in the metallic binding energy is given by the difference in the two peak split-points. The  $\text{Mn}2p$  peaks have an asymmetric shape for metal, which act as the primary XPS zone. Similarly, the  $\text{Ti}2p$  peaks adjust considerably to higher binding energy levels

compared to Mn with a binding energy value of about 20 eV. This is an indication that  $\text{Mn}^{3+}$  has been substituted for the  $\text{Ti}^{4+}$  cations in the sample. Since, the samples maintained a perovskite structure with rhombohedral symmetry, the Mn spectral region can be interpreted as the splitting characteristics in multiple component spectral lines form. This is a possible outcome which may be triggered by the coupling of non-oxidized  $3s$  electron with  $3d$  valence electrons in its lattice, which produces a doped material with improved features [31]. Fig. 2 (c) shows that the main peaks of  $\text{Mn}2p_{3/2}$  that corresponds to  $\text{Mn}^{3+}$  appear at 641.5 eV. This result was also determined by Gupta & Sen [32]. The lower shoulder that appears at 640.6 eV may correspond to the  $\text{Mn}^{2+}$  ( $2p_{3/2}$ ) level, which suggest the existence of a combination of both  $\text{Mn}^{3+}$  and  $\text{Mn}^{2+}$  ions [33, 34].

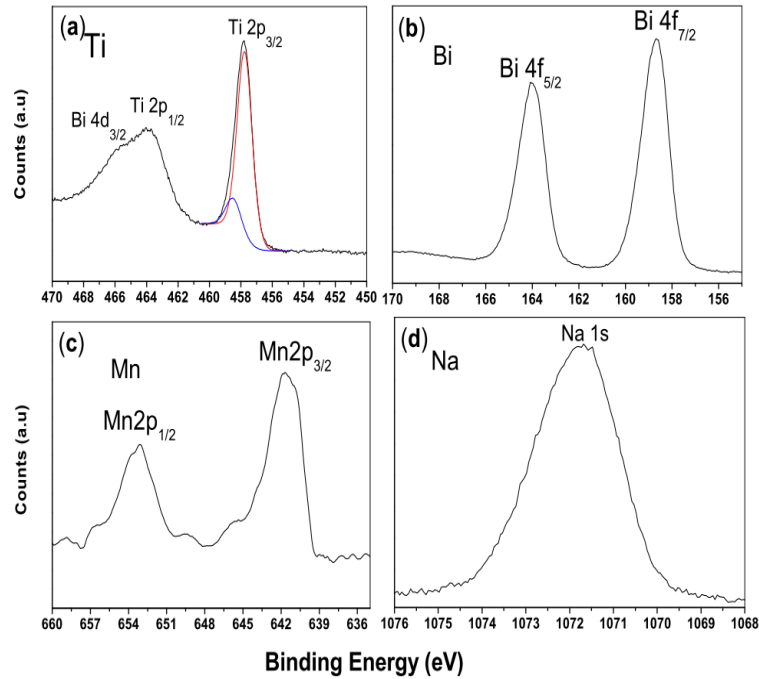


Fig 2. XPS spectra of BNTM-10 ceramic: (a)  $\text{Ti}2p$ ; (b)  $\text{Bi}4f$ ; (c)  $\text{Mn}2p$ ; (d)  $\text{Na}1s$ .

### 3.3. Ferroelectric Hysteresis (P-E) Loop

The polarization vs the electric field (P-E) hysteresis loops of the BNTM-2 & BNTM-10 ceramics at room temperature were characterized as shown in the Fig. 3. For the BNTM-2 sample, an ideal hysteresis loop was observed while the P-E loop was flattened and slanted as the maximum limit of 10% was approached for BNTM. BNTM-10 shows a very weak ferroelectric characteristic as clearly indicated in Fig. 3 (b). The oxygen vacancies created by  $\text{Mn}^{2+/3+}$  is likely responsible for this phenomenon. In addition, charge compensation will occur by the creation of oxygen vacancies. It is previously known that oxygen vacancies are the main cause of domain wall clamping, which leads to the weakening of polarization and ferroelectric properties [35]. The observed electrical properties seem to indicate that BNTM ceramics endure a phase transition at room temperature when the Mn content is increased to a higher level. However, the XRD data did not reveal any obvious phase transitions. The bipolar S-E curve exhibited a butterfly-shaped loop, with the typical domain switching identified in ferroelectrics and piezoelectric materials, observed for the BNTM-2 ceramics. This behavior diminishes with the doping of Mn at 10% as shown in the Fig. 3. For BNTM-10, the observed hysteresis loop is not associated with a ferroelectric material. Therefore, this behavior suggests that either the doped ceramics are still in the sub-switching regime even at a field strength of 40 kV/cm, or the ferro-electricity is largely suppressed. It is evident that the persistence of ferroelectricity results from the long rang polar order of the dipoles [36]. Any disruption in the polar order affects the ferroelectricity. Generally, a reduction of polarization occurs due to grain size reduction and the presence of structural imperfections such as oxygen vacancies and dislocations [37]. Due to the large leakage currents

caused by oxygen vacancies, ferroelectricity is deteriorated in BNTM-10. To stabilize the off-centering of titanium ( $\text{Ti}^{4+}$ ) ions which is important for ferroelectricity, an energy-lowering covalent bond is essential, which involve the empty d-orbitals of the transition metal ions. However, the higher substitution of  $\text{Ti}^{4+}$  ions by  $\text{Mn}^{3+/2+}$  ions disrupts the stabilization effect of the off-centering displacement, which weakens the polarization as shown in the P-E loops of BNTM-10.

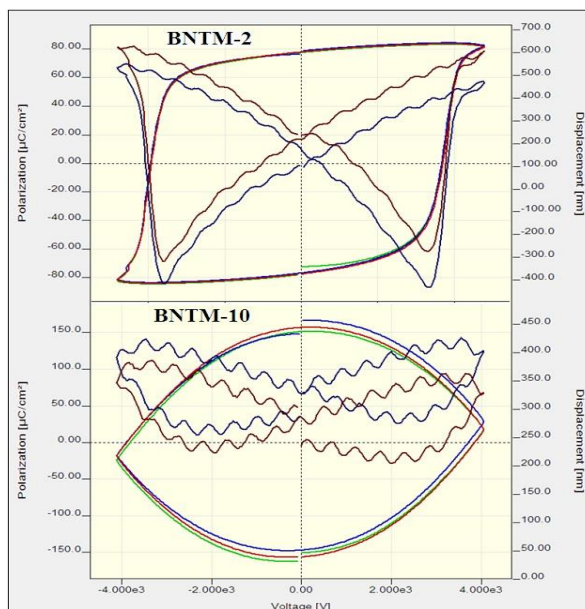


Fig 3. Ferroelectric polarization graph for BNTM-2 and BNTM-10

### 3.4. Magnetic measurements

Fig. 4 shows the graph of  $M(H)$  for the BNTM-10 sample and it is a typical paramagnet at a fixed temperature. The plot is linear, and the line intersects the origin of the graph. This behavior is associated with a paramagnet property and reversible magnetization (i.e. the same curve is obtained for either an increasing or decreasing field). This suggests that the magnetic susceptibility ( $\chi$ ) is an important property on this linear and reversible behavior of the  $M$ - $H$  curve [38]. Paramagnetism has many different origins. Since the  $M$ - $H$  curve is linear, two features are normally used to determine the origin of the paramagnetism. The first is the magnitude of  $\chi$  and the second is the temperature dependence of the susceptibility  $\chi(T)$ , as highlighted in Fig. 5.

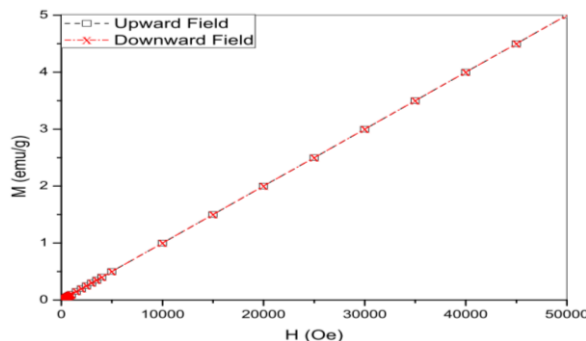


Fig. 4. Magnetization ( $M$ ) as a function of applied magnetic field ( $H$ ) for BNTM-10 at a fixed temperature. The squares (Black colour) represent data collected during the application of an increasing field and the  $x$ -symbols (Red colour) represent data collected as the field strength was decreased.

Fig. 5 (a) shows the graph of  $\chi(T)$  for BNTM-10 between 0–300 K exhibits a typical Curie-type paramagnet behavior. This type of magnetism may result from the presence of atoms with unpaired electrons. Curie-type paramagnetism has a particular temperature dependence  $\chi(T) = C/T$ , where  $C$  is a constant. A plot of  $1/\chi$  versus  $T$  is shown in Fig. 5 (b) for BNTM-10 between 0–300 K. This plot is very useful for characterizing Curie paramagnets. The slope of curve is equal to  $1/C$  and the Curie constant is given by following relation:

$$C = b\mu_{\text{eff}}^2 N \quad (1)$$

Where  $\mu_{\text{eff}}$  is the effective magnetic moment,  $b$  is a universal constant and  $N$  is the concentration of magnetic atoms with that moment.

The constant “ $C$ ” can be used to determine the product of the effective magnetic moment of an atom and the number of magnetic atoms present. If the number of magnetic atoms is known, it is then possible to determine the  $\mu_{\text{eff}}$  associated with the magnetic atoms.

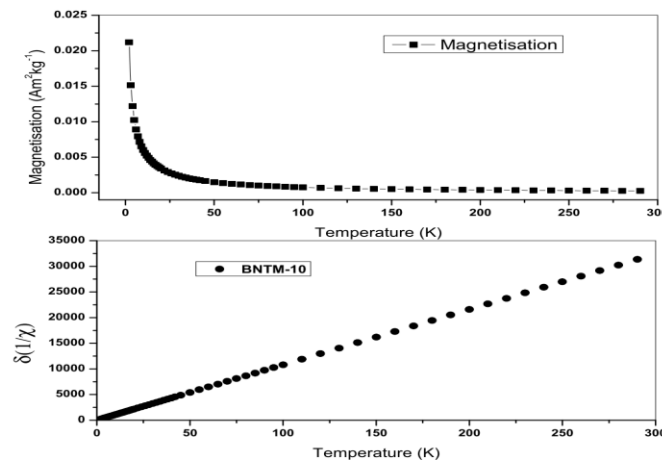


Fig. 5. Magnetic Susceptibility ( $\chi$ ) as a function of temperature ( $T$ ) at 100 G and 1 kG under the field-cooled (FC) and zero field-cooled (ZFC) conditions for BNTM-10

Fig. 6 shows the magnetic moment data collected by cooling the sample in zero applied magnetic field (ZFC), followed by the establishment of the magnetic field and the collection of magnetic moment data as the sample was warmed, followed by field cooling (FC). No hysteresis was observed for both FC and ZFC. Above the temperature of 100 K, the magnetization data can be fitted using the Curie-Weiss law and it was observed to rapidly increase below 50 K. At that temperature, the occurrence of a transition is indicated in the dielectric data measurement, as discussed in our recent study. The sudden increase of the susceptibility is either due to the result of the paramagnetic order of the BNTM-10 or to impurities and/or crystal defects, which can become dominant at low temperatures. In Fig. 6, the fitted Curie law for the lower range plot shows direct proportionality, which indicates that the magnetic susceptibility (denoted by  $\chi$ ) of a ferromagnetic material in the paramagnetic region is higher than the Curie point. The ferromagnetic characteristic is evident in Mn-doped BNT samples that were previously prepared for a separate investigation and is associated with the formation of bound magnetic polarons [39]. This is a confirmation that the perovskite structure indicated the existence of an incompatibility between ferroelectric materials and an abrupt magnetization in Mn-doped BNT ceramics. The super-paramagnetic nature is evident in the zero field-cooled sample, since a straight line graph is obtained. This is an indication of reduced resistivity of the Mn-doped material.

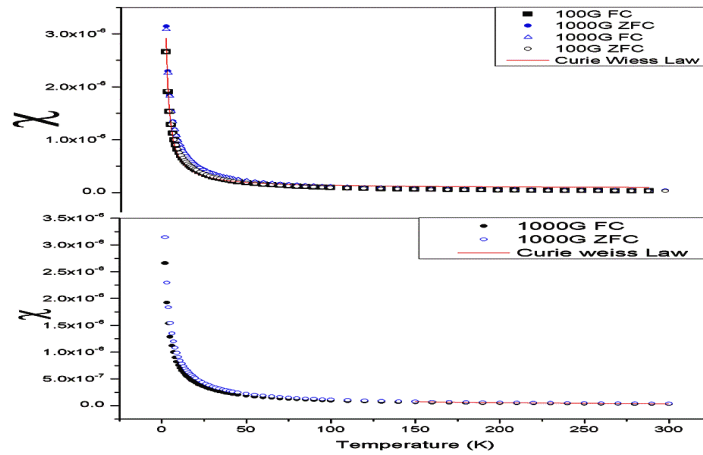


Fig. 6. Magnetic Susceptibility ( $\chi$ ) as a function of temperature ( $T$ ) at 100 G and 1 kG under the field-cooled (FC) and zero field-cooled (ZFC) conditions for BNTM-10.

The Curie-Weiss susceptibility is given by;

$$\chi_{cw} = C/(T - \theta) \quad (2)$$

where  $\theta$  is called the Curie-Weiss temperature and which is related to the strength of the interaction between moments, and its sign depends on whether the interaction helps to align adjacent moments in the same direction or opposite to each other. For  $\theta > 0$ , the interaction aligns adjacent moments in the same direction, while for  $\theta < 0$ , the interaction aligns adjacent moments opposite to each other. Fig. 7 shows the characteristic plot for the Curie behavior ( $1/\chi$ ) Vs temperature ( $T$ ), and the same is true for Curie-Weiss behavior. However, as shown in Fig. 7, instead of a straight line through the origin as observed in Fig. 5 (b), an x-axis intercept occurs at a positive or negative  $\theta$ . In the case of the ferromagnetic  $\theta$  ( $\theta > 0$ ), it can be seen that Eq. 2 diverges (goes to infinity) at  $T = \theta$ . This is the approximate location of a ferromagnetic transition, also known as the Curie temperature (denoted by  $T_C$ ). For an antiferromagnetic  $\theta$  ( $\theta < 0$ ), Eq. 2 will not diverge at  $T = \theta$ . However, the system may now have an antiferromagnetic transition, known as a Neel transition (denoted by  $T_N$ ), near  $T = \theta$ .

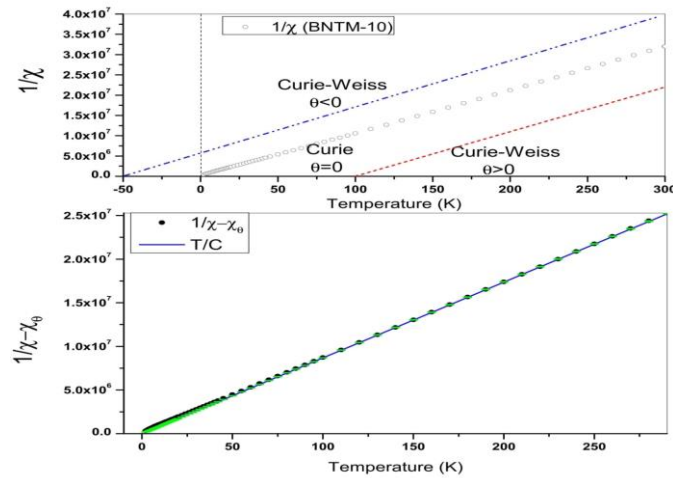


Fig. 7 The inverse of  $\chi$  as a function of  $T$  for a system exhibiting Curie ( $\chi = C/T$ ) and Curie-Weiss behavior ( $\chi = C/(T - \theta)$ ). When  $\theta > 0$ , the interaction between moments helps to align neighbouring moments in the same direction and when  $\theta < 0$ , the moments are aligned in opposite directions. When  $\theta = 0$ , the moments act completely independent of one another.

#### 4. Conclusions

In this research, the influence of changes in the oxidation number on the magnetic properties for manganese doping on the B-site of lead-free piezoelectric BNT ceramics were studied in detail. XPS results revealed the existence of  $\text{Mn}^{3+}$  along with the reduction of the valance of titanium ( $\text{Ti}^{4+}$ ) to  $\text{Ti}^{3+}$ . The  $\text{Mn}^{3+}$  ions play an important role of acceptor doping by substituting the  $\text{Ti}^{4+/3+}$  at the B-site and the formation of defect dipoles by creating oxygen vacancies in BNTM ceramics. The ferroelectric properties were improved by the addition of a small amount of Mn (only 2%) and deteriorate at the higher doping level of 10%. BNTM-10 exhibits obvious paramagnetism at low temperature. A paramagnetic exchange mechanism that involves a spin-polarized hole, trapped at Titanium vacancies is proposed and ascribed to the effective exchange interactions between the hole carriers and the magnetic Mn ions. These results are an important resource which can be consulted in the fabrication of Mn-doped BNT ceramics.

#### References

- [1] V. A. Isupov, *Ferroelectrics*, **315**, 123 (2005).
- [2] Y. Li, W. Chen, J. Zhou, Q. Xu, H. Sun, M. Liao, *Ceram. Int.* **31**, 31 (2005).
- [3] Z. H. Zhou, J. M. Xue, W. Z. Li, J. Wang, H. Zhu, J. M. Miao, *Appl. Phys. Lett.* **85**, 804 (2004).
- [4] R. A. Eichel, H. Kungl, *Funct. Mater. Lett.* **3**, 1 (2010).
- [5] E. Cross, *Nature* **432**, 24 (2004).
- [6] T. Takenaka, K. Maruyama, K. Sakata, *Jpn. J. Appl. Phys.* **30**, 2236 (1991).
- [7] R. B. Sun, Q. H. Zhang, B. J. Fang, J. iao, X. B. Li, *Appl. Phys. A* **103**, 199 (2011).
- [8] W. W. Ge, H. Liu., X. Zhao, W.Z. Zhong, *J. Alloys and Comp.* **462**, 256 (2008).
- [9] L. X. Zhang, W. Chen, X. Ren, *Appl. Phys. Lett.* **85**, 5658 (2004).
- [10] X. Ren, *Nat. Mater.* **3**, 91 (2004).
- [11] Q. Zhang, R.R. Whatmore, *J. Eur. Ceram. Soc.* **24**, 277 (2004).
- [12] H. Liu, W.W. Ge, X.P. Jiang, X.Y. Zhao, H.S. Luo, *Mater. Letter.* **62**, 2721 (2008).
- [13] Y. Guo, H. Fan, C. Long, J. Shi, L. Yang, S. Lei, *Jr. of Alloys and Compounds* **610**, 189 (2014).
- [14] T. Kimura, E. Fukuchi, T. Tani, *Jpn. J. Appl. Phys.* **44**, 8055 (2005).
- [15] H. Nagata, T. Shinya, Y. Hiruma, T. Takenaka, T. Sakaguchi, H. Haneda, *Ceram. Trans.* **167**, 213 (2005).
- [16] Y. S. Sung, J. M. Kim, J. H. Cho, T. K. Song, M. H. Kin, T. G. Park, **96**, 202901 (2010).
- [17] R. Zuo, S. Su, Y. Wu, J. Gu, M. Wang, L. Li, *Mater. Chem. Phys.* **110**, 311 (2008).
- [18] R. A. Sereay, W. Berlinger, K. A. Muller, R. W. Collins, *Phys. Rev. B* **16**, 4761 (1977).
- [19] T. Mikia, A. Fujimoto, S. Jida, *J. Appl. Phys.* **83**, 1592 (1998).
- [20] R. A. Eichel, R. Bottcher, *Mol. Phys.* **105**, 2195 (2007).
- [21] L. X. Zhang, E. Erdem, X. Ren, R. A. Eichel, *Appl. Phys. Lett.* **93**, 202901 (2008).
- [22] S. Stoll, A. Schweiger, *J. Magn. Reson.* **178**, 42 (2006).
- [23] K. A. Muller, *Phys. Rev. Lett.* **2**, 341 (1959).
- [24] H. Moriwake, C. A. J. Fisher, A. Kuwabara, *Jpn. J. Appl. Phys.* **49**, 09MC01 (2010).
- [25] K. A. Muller, W. Berlinger, J. Albers, *Phys. Rev. B* **32**, 5837 (1985).
- [26] E. Erden, P. Jakes, S. K. S. Parashar, K. Kiraz, M. Somer, A. Rudiger, R. A. Eichel, *J. Phys. Condens. Matter* **22**, 345901 (2010).
- [27] R. A. Eichel, P. Erhart, P. Traskelin, K. Able, H. Kungl, M. J. Hoffmann, *Phys. Rev. Lett.* **100**, 095504 (2008).
- [28] M. Ahart, M. somayazulu, R. E. Cohen, P. Ganesh, P. Dera, H. K. Mao, R. J. Hemley, Y. Ren, P. Liermann, Z. Wu, *Nature* **451**, 545 (2008).
- [29] C. Oliva, L. Forni, P. Pasqualin, A. D. Ambrosio, A. V. Vishniakov, *Phys. Chem* **1**, 355 (1999).
- [30] K. Siegbahn, C. Nordling, A. Fahlman, R. Nordbeng, K. Hemrin, J. Hedman, G. Johnsson, T. Bergmark, S.E. Karlsson, I. Lindgren, B. Lindberg, *Nova Acta Regiae Soc. Sci. Ups.*

- 4**, 20 (1967).
- [31] Q. Hang, W. Zhou, X. Zhu, J. Zhu, Z. Liu, T. Al-Kassab, J. Adv. Ceram. **2** (2013)
  - [32] P. R. Gupta, K. S. Sen, Phys. Rev. B, **10**, 71 (1974).
  - [33] D. Banerjee, H. W. Nesbitt, Am. Mineral **83**, 305 (1998).
  - [34] C. N. R. Rao, D. D. Sarma, S. Vasudevan, M. S. Hedge, Proc. R. Soc. A, **367**, 239 (1979).
  - [35] M. Wu, Y. Lu, Y. Li, J. Am. Ceram. Soc. **90**, 3642 (2007).
  - [36] M. Kuehn, H. Kliem, J. of Electrostatics **67**, 203 (2009).
  - [37] Z. Zhao, V. Buscaglia, M. Viviani, Phys. Rev. B **70**, 024 (2004).
  - [38] B. D. Cullity, Introduction to Magnetic Materials, Addison-Weley (1972),
  - [39] X. Tong, Y. Lin, S. Zhang, Y. Wang, C. Nan, J. Appl. Phy. **104**, 066108 (2008).